AIAA JOURNAL
Vol. 46, No. 5, May 2008

Application of Laminar-Turbulent Transition Criteria in Navier–Stokes Computations

J. Cliquet,* R. Houdeville,† and D. Arnal‡
ONERA, 31 055 Toulouse Cedex 4, France

DOI: 10.2514/1.30215

A new method concerning laminar-turbulent transition computation was implemented in the ONERA Reynolds-averaged Navier–Stokes solver elsA. It is based on the computation line concept and leads to the removal of most of the mesh topology limitations. Further improvements were also developed, such as the extension of a previous criterion (the Arnal–Habiballah–Delcourt criterion) to separated boundary-layers. Some changes in the numerical treatment of the transition point aimed at stabilizing and improving the accuracy of the computations. Two two-dimensional test cases [the Somers laminar airfoil and the A310 (TC11) profile] and a three-dimensional test case (the variable sweep angle wing) were considered to validate the implementation and the different improvements.

Nomenclature

a	=	sound speed
C_D	=	drag coefficient
C_f	=	skin friction coefficient $2\tau_w/\rho_\infty U_\infty^2$
C_L	=	lift coefficient
c	=	chord length
H_i	=	incompressible shape factor
L	=	reference length
l	=	mixing length
M	=	freestream Mach number
N	=	total amplification factor
P	=	pressure
Re_θ	=	Reynolds number based on momentum thickness and freestream conditions
Re_c	=	Reynolds number based on the chord length and freestream conditions
s	=	curvilinear abscissa
T	=	temperature
T_u	=	external turbulence level
x	=	streamwise coordinate
y^+	=	dimensionless wall distance
y	=	coordinate normal to the wall
z	=	spanwise coordinate
α	=	angle of attack
γ	=	intermittency function
ϵ	=	small parameter
θ	=	momentum thickness
$\underline{\Lambda}_2$	=	Pohlhausen parameter
Λ_2	=	mean Pohlhausen parameter
μ	=	viscosity coefficient
ρ	=	density
τ	=	total stress
ϕ	=	sweep angle
Ω	=	vorticity

Subscripts

cr	=	value at critical point location
eff	=	effective
i	=	stagnation conditions
l	=	laminar
T	=	value at transition location
t	=	turbulent
w	=	value at the wall
δ	=	value at boundary-layer edge
∞	=	conditions at upstream infinity

I. Introduction

THE use of computational fluid dynamics (CFD) tools based on Reynolds-averaged Navier–Stokes (RANS) solvers able to handle flows with laminar-turbulent transition in an automatic and autonomous way is of primary interest in the world of aerospace industry. Practically, it is not always possible to obtain reliable results for wing or airfoil design, without taking into account the laminar-turbulent transition process. To this end, several attempts to include transition computation into RANS solvers were carried out in recent years. Wilcox [1] proposed the use of low Reynolds number turbulence models. This offers implementation facilities but cannot cover the wide range of phenomena involved in transition. Menter et al. [2–4] proposed the use of transport models for the intermittency and for the momentum thickness Reynolds number. Its field of application was originally limited to bypass transition but was extended to transition triggered by instabilities [5] and represents a very promising strategy. Two other popular approaches are the coupling of a RANS solver with a boundary-layer code [6] and the direct introduction of transition criteria into RANS solvers. The former strategy overcomes the lack of precision usually observed on boundary-layer velocity profiles in RANS solvers without the need of high mesh refinement. The main difficulties are the extraction from the Navier–Stokes solver of the boundary conditions for the boundary-layer solver, the coupling process between two different solvers, and the boundary-layer separation treatment. The latter strategy is more straightforward provided that the precision problem is solved, and is the one that has been retained in the ONERA RANS solver elsA.

The present paper presents the implementation of a new computation line concept in the elsA Navier–Stokes solver and gives some applications for two-dimensional (2-D) and three-dimensional (3-D) flows. A new transition criterion gathering the previous Arnal–Habiballah–Delcourt (AHD) and Gleyzes–Habiballah (GH) criteria is also presented. The main interest of this new criterion is to cope with a large range of pressure gradient parameters from accelerated flows to separation bubbles. These modifications have already been partly validated on simple 2-D geometries at low Mach numbers [7].

Presented as Paper 515 at the 45th AIAA Aerospace Meeting and Exhibit, Reno, NV, 8–11 January 2007; received 8 February 2007; revision received 1 August 2007; accepted for publication 19 December 2007.

*Ph.D. Student, Aerodynamics and Energetics Modelling Department, 2 Avenue Edouard Belin, BP 4025; Julien.Cliquet@onera.fr.

†Research Engineer, Aerodynamics and Energetics Department, 2 Avenue Edouard Belin, BP 4025; Robert.Houdeville@onera.fr.

‡Research Engineer, Aerodynamics and Energetics Department, 2 Avenue Edouard Belin, BP 4025; Daniel.Arnal@onera.fr.

It must be noted that the approach is not limited to 2-D flows, and crossflow instability modes (not considered in this paper) are also taken into account in the elsA solver with a simple criterion based on the displacement thickness in the crossflow direction. Validation test cases are compared with experimental results and boundary-layer solutions. The 2-D test cases are the laminar "Somers" airfoil and the A310 profile in takeoff configuration (TC11) which was used as a test case within the framework of the EUROLIFT European funded program [8]. The 3-D test case is the AFV swept wing (Aile à Flèche Variable, French acronym for variable sweep angle wing) which was also used in the EUROLIFT project.

II. Numerical Aspects

A. Presentation of the elsA Software

The ONERA elsA software [9] is based on an object-oriented programming technique. It solves the Navier–Stokes equations on structured meshes with a cell-centered finite volume discretization technique. All of the results which are presented here were obtained using a time integration scheme of backward Euler type, with a local time step and a scalar lower–upper symmetric successive overrelaxation (LU-SSOR) method for the implicitation. For the space discretization, the Jameson centered scheme is used. It is stabilized by a blend of second and fourth difference artificial dissipation with Martinelli correction. The corresponding χ_2 and χ_4 coefficients are generally taken equal to 1 and 0.016. The transition computation relies on the effective viscosity concept $\mu_{\text{eff}} = \mu + \gamma\mu_t$, where γ is an intermittency function.

B. Boundary-Layer Thicknesses

In the boundary-layer approach, the velocity U_δ at the boundary-layer edge is constant with y. The boundary-layer thickness δ is defined as the distance to the wall, which verifies

$$\left(\frac{u}{U_\delta}\right)_\delta = 0.99 \tag{1}$$

In the Navier–Stokes approach, the velocity outside of the boundary-layer still varies more or less as a function of y. This is due to the presence of a pressure gradient in the direction normal to the wall. The formula commonly used in the boundary-layer approach is then not applicable because U_δ is not known.

Another estimation method can be used relying on the boundary-layer definition. At the boundary-layer edge, the shear stress τ must become small. The total shear stress is defined as $\tau_{\text{tot}} = \tau_l + \tau_t$; τ_l and τ_t can be expressed in the following approximated way:

$$\tau_l = \mu|\Omega| \quad \text{and} \quad \tau_t = \mu_t|\Omega| \tag{2}$$

where $\mu_t \sim l^2|\Omega|$, where l is the mixing length, which means that τ_t decreases as $|\Omega|^2$ at the boundary-layer edge. The use of τ_{tot} improves the definition of δ in the turbulent regions but changes nothing in the laminar regions. The criterion allowing one to detect δ in elsA is finally the following. The valuesδ_Ω and δ_τ are obtained by interpolation between the points of the lines in such a way that

$$\frac{|\Omega|_\delta}{|\Omega|_{\max}} = \varepsilon_\Omega \quad \text{gives } \delta_\Omega \tag{3}$$

$$\frac{|\tau|_\delta}{|\tau|_{\max}} = \varepsilon_\tau \quad \text{gives } \delta_\tau \tag{4}$$

$$\delta = \min(\delta_\Omega, \delta_\tau) \tag{5}$$

The ε_Ω and ε_τ parameters are two small values of the order 0.001 and 0.015, respectively. To ensure that ε_τ does not mask ε_Ω in the laminar regions, ε_τ is weighted with the intermittency function γ: $\varepsilon = \gamma\varepsilon_\tau + (1-\gamma)\varepsilon_\Omega$. $|\Omega|_{\max}$ and $|\tau_{\text{tot}}|_{\max}$ are searched along the lines normal to the wall, whose length is defined by the geometric dependence domain Δ of the wall. For monoelement configurations, Δ is the distance between the wall and the outer boundary of the computation domain. This distance can be large compared to δ. For multi-element configurations, Δ corresponds to the equal distance to two opposite walls. If $|\Omega|$ reaches several minima along the lines normal to the wall, the boundary-layer thickness estimation can be wrong. No problem would be encountered if it was sufficient to take the first one. But if a boundary-layer separation appears, the vorticity $|\Omega|$ reaches zero at the minimum of velocity in the separation zone. To avoid an underestimation of δ, a first solution is to introduce the mean velocity $\rho|U|$ defined on a length Δ normal to the wall:

$$\overline{|\rho U|} = \frac{1}{\Delta}\int_0^\Delta \rho|U|\mathrm{d}y \tag{6}$$

The values δ_Ω and δ_τ will be searched in the region as $\rho|U| > 0.4\overline{\rho|U|}$ to avoid the near-wall region and the backflow region. A second solution consists of making an approximated estimation of δ. According to Stock and Haase [10], the boundary-layer thickness is located near the point where the quantity $(y\Omega)$ is maximum. A new problem can appear when the length Δ of the line is very large compared to δ. In the presence of a pressure gradient in the direction normal to the wall, $|\Omega|$ is nearly constant on a large distance and the quantity $(y\Omega)$ increases as the distance to the wall far from δ. A solution is to limit the length of the normal lines using the user interface. Another solution consists of trying to reduce the influence of the quantity $(y\Omega)$ when Ω is constant. A weighted mean vorticity is defined on the length Δ normal to the wall:

$$\overline{|\Omega|} = \frac{1}{\Delta^2}\int_0^\Delta |\Omega| y\,\mathrm{d}y \tag{7}$$

The point y_0 corresponding to the maximum of $(|\Omega| - \overline{|\Omega|})y$ is then searched and δ is sought hereafter this point. The subtraction of $\bar{\Omega}y$ allows one to reduce the problem linked to the pressure gradient normal to the wall. Another problem appears when the two parameters ε_τ and ε_Ω are never reached. In that case, a solution consists in admitting that δ is reached if U decreases when y increases.

C. Computation Line Concept

For integral thicknesses and nonlocal transition criteria application, a common concept comes to light, that of computation line. Such a line is built on a set of points which can be described from both directions. At each point, the access to a certain number of physical values such as cell or node center coordinates, wall distance, conservative variables, and other derived quantities has to be provided.

It has been chosen to clearly separate 1) the boundary-layer treatment from 2) the line construction from 3) the interpolation of values in the computation mesh. This enables relatively distinct evolutions of points 2 and 3 with respect to point 1. It also offers the possibility of providing a much clearer implementation and is then much easier to maintain. The principle of the implementation uses the following objects of object-oriented programming:

1) The "line" object contains information to compute a set of lines, either all normal lines starting on a given wall boundary for integral thicknesses computation or all transition lines starting in a wall window[§] containing stagnation points or attachment lines. This object is not limited to a single domain and contains all topological mesh information to compute the lines and retrieve flow data quantities. Each line can be scanned using simple loops. Each line object holds a "container" to store flow data.

2) The container object contains flow data in specific arrays organized to be easily traveled through by simple loops along lines.

3) The "thickness" object integrates the velocity profiles. It is associated with a "normal line" object and a container.

4) The "transition" object computes and applies transition criteria. It is associated with a "transition line" object and a container.

[§]Face or subface of domain coinciding with a wall.

Contrary to the normal line object, the transition line object must contain information to go from wall cell faces to container to compute criteria, and from container to wall cell faces to apply the transition results. Such an organization is represented in Fig. 1.

D. Some Remarks About the Implementation

With the proposed implementation, the principle of transition computation is the following. User interface provides the origins of the transition lines, wall by wall. In a first step, the integral thicknesses are computed on all the concerned walls by a thickness object which integrates the velocity profiles. This object is associated to a normal line object and a container to store the results of the integration. The transition computation principle is outlined in Fig. 1. The flow data are initially stored in the elsA intrinsic data structure (cells/domains). Each wall window containing at least a transition line section is associated to a container object which saves the data necessary for transition computation in a wall window structure. These data are then transferred into an array built in a global line structure, thanks to topological information provided by the transition line object. These in-line data, which are, for example, the integral thicknesses, the external turbulence level, or the Pohlhausen parameter Λ_2, are provided to the transition object, whose function is to apply the criteria as an input. As a result, the intermittency function is computed in an in-line structure. The last step of the process is to rearrange the intermittency in the initial wall window structure, still by using the "elementary transition line" object, allowing one to apply the results of transition computation.

E. Transition Criterion

For the streamwise instability mode, the most frequently used criterion in boundary-layer computations is the e^N method [11,12] combined with Mack's relationship for 2-D incompressible flows [13]:

$$N_T = -2.4\ \ell_n(T_u) - 8.43; \qquad T_u < 2.7\% \tag{8}$$

where T_u is the freestream turbulence level. Such a method needs direct linear stability computations or the use of a database method. The transition criterion used for the present Navier–Stokes computations is a blending of existing criteria to cover the full range of pressure gradients which can be encountered over airfoils. For moderate pressure gradients, the AHD criterion [14] is well suited to predict the onset of the transition for small or moderate T_u levels. This criterion is based on the linear stability theory for flows with low freestream turbulence levels. It was originally developed for incompressible flows ($M < 0.6$) over adiabatic walls but has recently been extended to compressible flows.

The basic idea is to use the Falkner–Skan self-similar solutions to represent the laminar boundary-layer profiles, which are characterized by the local Pohlhausen parameter Λ_2. For each solution, the total amplification coefficient can be expressed by

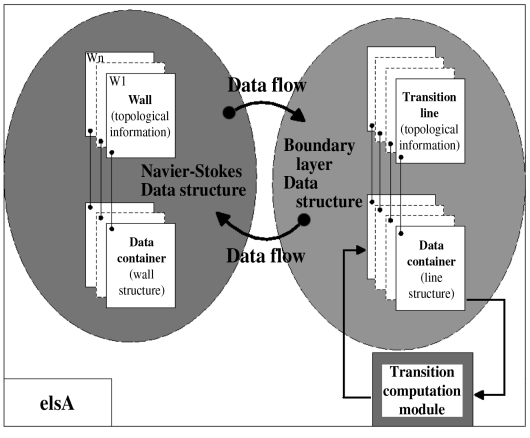

Fig. 1 Organization of transition computation in elsA.

$$\mathbf{N}\,(Re_\theta - Re_{\theta_{\rm cr}}, \Lambda_2); \qquad Re_\theta = \frac{U_e\theta}{\nu}; \qquad \Lambda_2 = \frac{\theta^2}{\nu}\frac{\mathrm{d}U_e}{\mathrm{d}s} \tag{9}$$

in which $Re_{\theta_{\rm cr}}$ is the critical Reynolds number based on the momentum thickness θ at the point where unstable disturbances start to develop. Although the preceding relationship is strictly valid for self-similar boundary layers, it is extended to actual flows by replacing Λ_2 with its mean value $\bar{\Lambda}_2$ along the streamline corresponding to the region where the boundary-layer is unstable:

$$N = N(Re_\theta - Re_{\theta_{\rm cr}}, \bar{\Lambda}_2); \qquad \bar{\Lambda}_2 = \frac{1}{s - s_{\rm cr}}\int_{s_{\rm cr}}^{s} \Lambda_2\,\mathrm{d}s \tag{10}$$

The transition location is characterized by

$$\begin{cases} N = N_T \\ Re_\theta = Re_{\theta T} \end{cases} \tag{11}$$

Combining Eq. (9) written at the transition location and Mack's relationship Eq. (8), N_T can be eliminated. The AHD criterion is then based on the following relationship

$$N(Re_{\theta T} - Re_{\theta{\rm cr}}, \bar{\Lambda}_{2T}) = N_T \tag{12}$$

Taking Eq. (8) into account, Arnal [14] proposed the analytical form of the criterion:

$$Re_{\theta T} - Re_{\theta{\rm cr}} = -206\exp(25.7\bar{\Lambda}_{2T})[\ell_n(16.8T_u) - 2.77\bar{\Lambda}_{2T}] \tag{13}$$

The two parameters $Re_{\theta T} - Re_{\theta{\rm cr}}$ and $\bar{\Lambda}_{2T}$ were previously introduced by Granville [15] for his criterion based on a correlation of experimental results for small turbulence levels, on the order of 0.1%. Contrary to the Granville criterion, the relationship Eq. (13) relies on a theoretical basis and includes the T_u effect.

For practical applications, $Re_{\theta{\rm cr}}$ must be known, as well as the abscissa $s_{\rm cr}$ from which unstable frequencies start being amplified. From stability computations, the following expression was obtained:

$$Re_{\theta{\rm cr}} = \exp\left[\frac{52}{H_i} - 14.8\right] \quad \text{for } 2.2 < \mathrm{H}_i < 4 \tag{14}$$

For $Re_\theta < Re_{\theta{\rm cr}}$, the boundary layer remains stable. The values $s_{\rm cr}$ and $Re_{\theta_{\rm cr}}$ are obtained when $Re_\theta = Re_{\theta_{\rm cr}}$.

To take into account highly positive pressure gradients leading to boundary-layer separation and beyond, another criterion previously proposed by Gleyzes et al. [16] and Habiballah [17] (GH) is used. This criterion is based on the fact that near separation and beyond, the amplification rates of unstable frequencies are almost independent of the frequency, but only depend on the shape parameter of the velocity profile and on the Reynolds number based on the momentum thickness. It uses exact stability computations for the separated Falkner–Skan self-similar solutions and takes the form

$$N(s) - N(s_1) = \int_{Re_{\theta_1}}^{Re_\theta} \frac{-2.4}{B(H_i)}\,\mathrm{d}Re_\theta \tag{15}$$

with

$$B = \begin{cases} \frac{-162.11093}{H_i^{1.1}} & \text{if } 3,36 < H_i \\ -73\exp[-1,56486(H_i - 3,02)] & \text{if } 2.8 < H_i < 3,36 \\ -103\exp[-4,12633(H_i - 2,8)] & \text{if } H_i < 2,8 \end{cases} \tag{16}$$

In relation (15), $N(s_1)$ is the total growth rate at s_1 where $\theta = \theta_1$. The value s_1 must be chosen in the region where the basic hypothesis upon which this criterion is based on holds, which means for values of H_i larger than 2.7 or 2.8 (it has been verified that the AHD and GH criteria give similar results for this range of shape factors corresponding to mild positive pressure gradients). $N(s_1)$ is obtained by inverting relation (13) of the AHD criterion.

F. Intermittency Function

Imposing a step from zero to one to the intermittency function at the transition location can lead to oscillations on the momentum thickness which can create numerical difficulties. Moreover, the AHD criterion gives the point where $\bar{u}'^2$ starts to increase, which is upstream of the point where C_f starts to increase. To cope with these two problems, and also with the systematic overestimation of Re_θ in the Navier–Stokes solvers, the transition point location given by the criteria is first shifted downstream by ΔX using an extrapolation of $Re_\theta(X)$ in the laminar region, such as ΔX corresponds to ΔRe_θ on the order of 10% of Re_θ. Then, a simple intermittency function of the form

$$\gamma = \frac{1}{0.15^2}\left[\frac{Re_\theta - Re_{\theta T}}{Re_{\theta T}}\right]^2 \tag{17}$$

is applied. The intermittency function γ reaches one as soon as $Re_\theta(X)$ has increased by 15%. In this formulation, the Re_θ value is not the actual value given by the solution but the extrapolated value from the laminar region. This may significantly improve the stability of the iterations. This also improves significantly the physics of the solution near the transition point. However, the proposed intermittency function does not pretend to model the physics of the intermittency region. This is a much more difficult problem, especially when associated with transport equations for the turbulence models.

G. Implementation of the Transition Criterion in the elsA Software

Equations (14) and (15) are very sensitive to the value of the shape parameter H_i. To overcome the precision problem on that parameter in RANS computations, H_i is expressed as a function of Λ_2 with the following formula:

$$H_i = 4.02923 - \sqrt{-8838.4\Lambda_2^4 + 1105.1\Lambda_2^3 - 67.962\Lambda_2^2 + 17.574\Lambda_2 + 2.0593} \tag{18}$$

To avoid numerical difficulties in computing Λ_2, which needs to know $\mathrm{d}U_e/\mathrm{d}x$ at the boundary-layer edge, this last quantity is obtained from $\mathrm{d}p/\mathrm{d}x$ at the wall (according to first-order boundary-layer theory). The use of this criterion needs to follow a particular direction to first detect the critical point and then to compute the integral Eq. (15). Once the transition point is determined, the boundary-layer is imposed turbulent when the intermittency function reaches the value of one.

III. Applications

A. Somers Airfoil

This profile was developed around 1960 within the framework of natural laminar flows (NLF) airfoils research for sailplanes. It became a popular test case for transition computations because of these characteristics. The aerodynamic conditions that were applied here correspond to a Mach number of 0.1, a temperature of 285 K, and a unit Reynolds number of 4.0×10^6 m^{-1}. The mesh is issued from a mesh convergence study and is made of one block containing 439×161 nodes (Fig. 2). The y^+ value of the first cells above the wall is on the order of one. The AHD-GL criterion was used with the experimental freestream turbulence level $T_u = 0.03\%$. Numerical results obtained from computations were compared with experimental data obtained in the NASA Langley Research Center's low-turbulence pressure tunnel [18]. The experimental and computed transition locations (before the shifting) were compared on the suction side of the airfoil for several angles of attack (Table 1). One can observe that elsA detects transition slightly upstream of the experimental values. This is due to the overestimation of the integral thicknesses generally encountered in RANS computations and validates the shifting of the transition location. A range of angles of attack $-4 < \alpha < 12$ deg was studied to compare the experimental and computed polar curves (Fig. 3a). The results obtained with a fully turbulent computation are also plotted in the figure. One can notice a significant improvement in the polar curve prediction using the transition criterion. A factor of two on the drag coefficient distinguishes fully turbulent results from results obtained with the transition criterion in the range of lift coefficient $0.2 < C_L < 0.8$. A comparison between results obtained with the elsA software and the ONERA boundary-layer code 3C3D [19,20] on the skin friction coefficient is plotted in Fig. 3b. The transition treatment in the boundary-layer code 3C3D is based on a mixing layer scheme combined with an intermittency function, which has been calibrated on 2-D experiments at zero and positive pressure gradients to model the C_f distribution including the overshoot on C_f [14]. One can notice that the boundary-layer computation stops because of the occurrence of the boundary-layer separation at about 42% of the chord. The elsA computation is in good agreement with the boundary-layer computation in the laminar region and is able to reach convergence using the extended AHD criterion. The laminar separation bubble does not appear in the elsA computation because transition occurs just upstream and is detected by the AHD part of the combined criterion. For higher angles of attack, transition is detected by the GH part of the criterion.

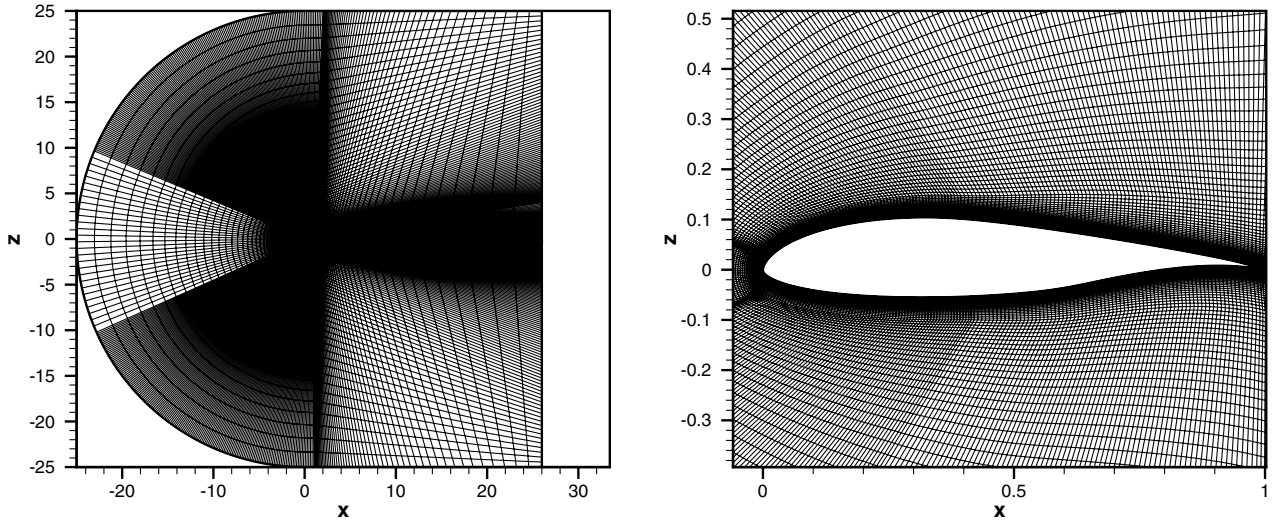

a) Entire domain

b) Zoom on airfoil vicinity

Fig. 2 Somers airfoil mesh.

Table 1 Comparison between experimental and computed transition location on the suction side of the airfoil

Angle of attack	$x/c\|_{tr}$ elsA	$x/c\|_{tr}$ exper.
−4 deg	0.44	0.46
−2 deg	0.40	0.42
0 deg	0.37	0.38
2 deg	0.33	0.35
4 deg	0.24	0.27

B. A310 Profile

The second test case is the A310 profile (TC11) in takeoff configuration, taken at 59% of the span. It represents an interesting test case because of the complex phenomena that can occur on that kind of high-lift configuration. The mesh presented in Fig. 4a was generated within the framework of a GARTEUR group (Group for Aeronautical Research and Technology in Europe) and is made of 84,400 nodes divided into eight domains around the profile and a C-block in the outer part. It is extremely deformed around the trailing edges of the three elements. These refined zones are the consequence of the distribution of the points on the surfaces and do not necessarily cover the strong gradients zones where a fine mesh is required. It can also be observed that the mesh lines normal to the joints between the domains contain discontinuities around the leading edge which leads to a deformed mesh. The experiments were carried out in the ONERA F1 wind tunnel [21]. To simulate takeoff conditions, a Mach number $M_\infty = 0.2$ and an angle of attack $\alpha = 21.4$ deg were used. The Reynolds number based on the airfoil chord was fixed to $Re_c = 6 \times 10^6$. The experimental freestream turbulence level [22], equal to 0.05%, was used for the computation and the stagnation temperature was fixed to 290.3 K. Adiabatic wall conditions on both sides of the three elements and a nonreflecting condition with uniform flow at infinity were applied. Smith's $k - l$ [23] turbulence model was used with the AHD-GL criterion (see Sec. II.E) and the parabolic intermittency function (see Sec. II.F). The transition location is computed on both sides of the three elements.

1. Comparison with Experimental Results

The experimental and computed pressure coefficients are plotted in Fig. 4b. The comparison reveals a good agreement. Results from a fully turbulent computation are also plotted as dotted lines. One can notice that on the slat, at the front of the main wing, and on the flap, the C_p values with transition are lower than the fully turbulent ones. The effect is favorable with respect to the experimental results, except on the flap. This can be due to the displacement thickness δ_1 which is lower when transition is taken into account, leading to a less significant decrease of the effective curvature. Figure 5 shows a comparison between a fully turbulent computation and a computation with transition on the skin friction coefficient. In the laminar zone of the suction sides, the skin friction coefficient of the computation with transition is equal to about 30% of the fully turbulent value. On the pressure side, the same kind of effect can be observed in the zones where the fully turbulent computation is well established. After the transition point, on the suction side, the skin friction coefficient of the computation with transition exceeds the turbulent values. This is an effect of the velocity profile evolution in the boundary-layer which is more developed in the fully turbulent case and leads to lower wall velocity gradients.

2. Comparison with Boundary-Layer Computations

Comparisons between results obtained with elsA and results obtained with the ONERA 3C3D boundary-layer code (see Sec. III.A) initialized with the elsA wall pressure distribution are shown. A stagnation pressure $p_i = 1.026910^5$ Pa and a stagnation temperature $T_i = 293.2$ K deduced from the elsA computation conditions were used to preserve the Reynolds number based on the airfoil chord, and a database method [24] is used for transition purposes.

Table 2 gives an overview of the predicted transition locations. The elsA and 3C3D computations reveal that the pressure side of the three elements are fully laminar. This agrees with the C_p distribution (see Fig. 4b) which emphasizes the continuous flow acceleration up to the trailing edges of the main wing and the flap. It can be noticed that the increasing pressure zone, which occurs at $x/c = 0.8$, is located under the recirculation zone and does not influence the boundary layer. On the suction side of the slat, the two approaches give exactly the same predictions, which is in agreement with the strong pressure gradient located downstream of the suction peak. The 3C3D code detects laminar boundary-layer separation which reveals the presence of a transition bubble. On the suction side of the main wing, transition is triggered by the surface slope discontinuity. Whereas, elsA immediately detects transition, 3C3D detects

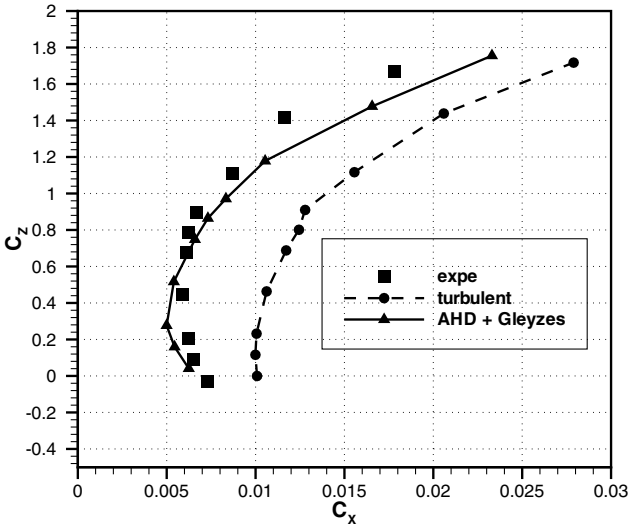

a) Comparison between elsA computation and experimental data on the polar curve

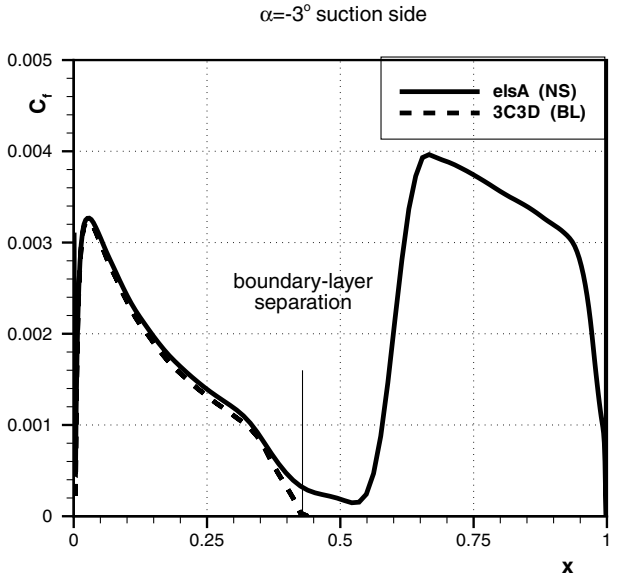

b) Comparison between elsA computation and boundary layer computation (3C3D) on the skin friction coefficient for an angle of attack of −3°

Fig. 3 Somers airfoil.

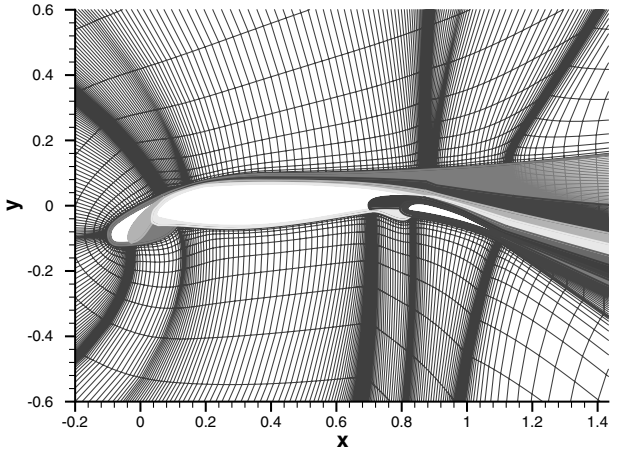

a) A310 mesh from the GARTEUR group

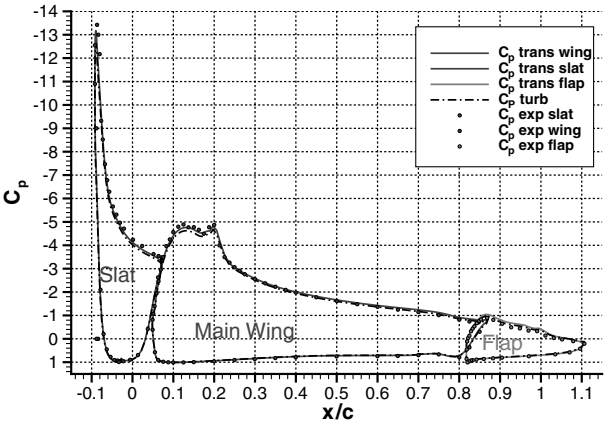

b) Comparison between experimental and computed pressure distributions on the A310 profile

Fig. 4 A310 profile.

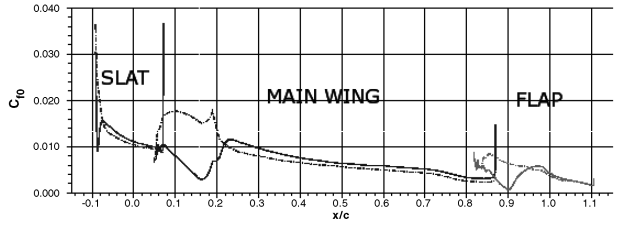

a) Suction side

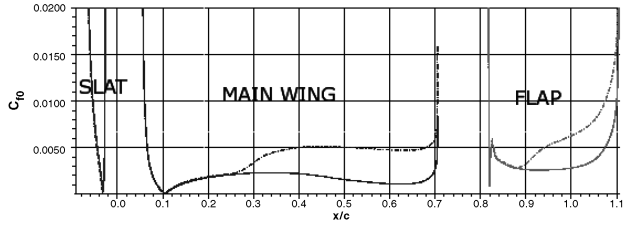

b) Pressure side

Fig. 5 Comparison between fully turbulent computation (dashed lines) and computation with transition (solid lines) on the skin friction coefficient C_{f0} of the A310 profile.

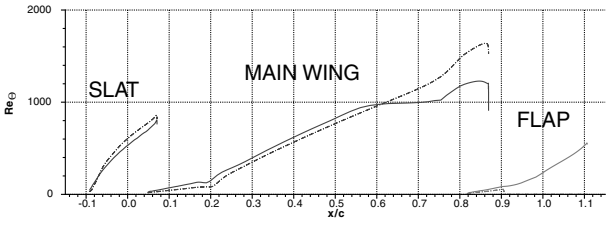

a) Suction side

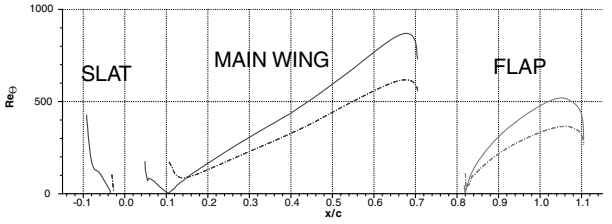

b) Pressure side

Fig. 6 Comparison between boundary-layer (dashed lines) and elsA (solid lines) computation with transition for the Reynolds number based the momentum thickness Re_θ of the A310 profile.

transition a few nodes downstream. On the flap, elsA detects transition just downstream of the strong acceleration zone; 3C3D detects a boundary-layer separation.

Figure 6 focuses on the momentum thickness Reynolds number. On the main wing, an overestimation of the Reynolds number based on the momentum thickness Re_θ of 15% can be observed up to $x/c = 0.25$. On the slat, the integral thicknesses are slightly overestimated in elsA with respect to 3C3D results up to $R_\theta = 2000$, which means in the laminar zone. The fact that the difference between the two approaches is weaker than on the main wing can be due to the strong acceleration of the flow at the leading edge of the slat. On the pressure side, both approaches stay fully laminar on the three elements and the overestimation of Re_θ is between 15 and 20%. Figure 7 shows a comparison between the skin friction coefficient obtained with the boundary-layer computation and the one obtained with elsA. A good agreement can be noticed. The discrepancies between elsA and 3C3D results are lower than 10% on a large part of the three bodies. The highest difference is located on the suction side of the slat and just upstream of the transition location on the main wing. The large oscillation of the 3C3D result at $x/c = 0.21$ is due to the geometrical discontinuity on the suction side of the airfoil, which leads to an oscillation on the pressure distribution used as input for the boundary-layer computation. On the suction side of the flap, 3C3D detects laminar boundary-layer separation at $x/c = 0.9$. This is the location where elsA detects boundary-layer transition. Upstream of this point, a good agreement can be observed.

Table 2 Transition location computed with elsA and 3C3D

Wing element	$x/c\|_{tr}$ elsA	$x/c\|_{tr}$ 3C3D
Slat suction side	−0.08	−0.08
Main wing suction side	0.19	0.22
Flap suction side	0.89	0.91
Slat pressure side	fully laminar	fully laminar
Main wing pressure side	fully laminar	fully laminar
Flat pressure side	fully laminar	fully laminar

C. Variable Sweep Angle Wing

The AFV research wing was chosen as a 3-D test case because it presents a double interest. First, its mesh contains most of the difficulties that the new implementation previously presented has to overcome while remaining relatively simple because only five faces of domains (the slat suction side, the main wing suction and pressure sides, and the flap suction and pressure sides) are concerned with transition computation. The second interest is that this wing in high-lift configuration was extensively studied in the ONERA F1 wind tunnel within the framework of the EUROLIFT project to constitute a large database for the validation of the results [8,25,26]. Many numerical

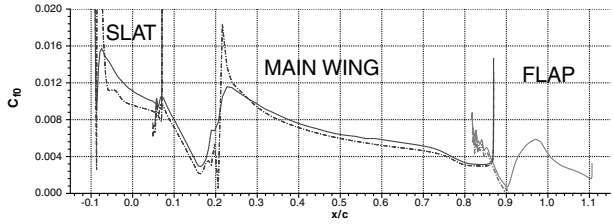

a) Suction side

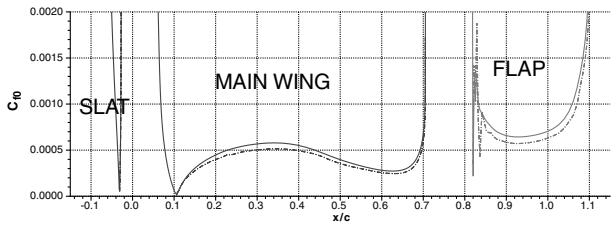

b) Pressure side

Fig. 7 Comparison between boundary-layer computation (dashed lines) and elsA computation (solid lines) with transition for the skin friction coefficient C_{f0} of the A310 profile.

results are also available. The AFV model is a rectangular untwisted wing made of 1) a slat leading edge ($\delta_{\text{slat}} = 30$ deg), 2) a main wing, the two-dimensional shape of which is the RA16SC1 profile with a chord equal to 0.5 m in the direction normal to the leading edge, and 3) a flap ($\delta_{\text{flap}} = 20$ deg). Tests carried out within the EUROLIFT program considered two sweep angles, $\phi = 30$ and $\phi = 40$ deg. The results presented here are based on the case $\phi = 40$ deg only with a wing span equal to 2 m (from tunnel floor to wing tip). The mesh contains 3.073×10^6 nodes distributed in 40 blocks, including 12 blocks around the model as represented in Fig. 8. The boundary conditions for the computation are adiabatic wall and uniform flow at infinity (nonreflecting condition). The floor of the wind tunnel is replaced by a symmetry condition. The aerodynamic conditions are $M_\infty = 0.2$ and $T_\infty = 299.5$ K. Transition is computed with the AHD criterion and a freestream turbulence level of $T_u = 0.1\%$. The turbulence model used is the $k - l$ model of Smith [23].

1. Variation of the Angle of Attack

Six angles of attack were considered: $\alpha = 5$, $\alpha = 15$, $\alpha = 17.5$, $\alpha = 22.5$, $\alpha = 25$, and $\alpha = 30$ deg. The aim here is to verify the

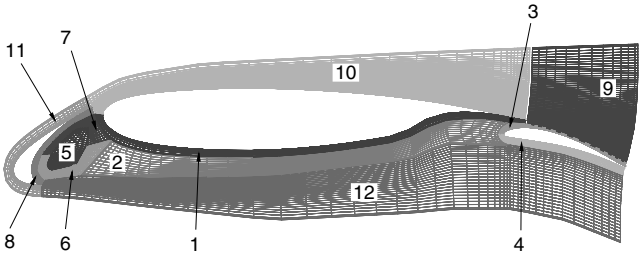

Fig. 8 Mesh and block indexing of the internal region of the AFV configuration (one point over two).

robustness of the developments concerning transition computation in elsA in the case of a 3-D configuration. Figure 9a shows a comparison between the experimental and computed evolutions of the lift and drag coefficients with the angle of attack. The results are in good agreement for the six angles of attack. No significant difference can be emphasized between fully turbulent computations and computations with transition. The evolution of the transition location on the upper side of the slat, $Re_c = 2.8 \times 10^6$, with the angle of attack, is as follows: $\alpha = 15$, 17.5, and 22.5 deg, and $X_T/c = 0.06$, 0.02, and 0.01. The case corresponding to $\alpha = 5$ deg is not considered because it is fully laminar, and the cases corresponding to $\alpha = 25$ and $\alpha = 30$ deg because they are fully turbulent. The upstream displacement of the transition location on the upper side of the slat with the increase of angle of attack is clear. Figure 9b shows the polar curve for a higher value of the Reynolds number $Re_c = 5.9 \times 10^6$. This time, angles of attack between 5 and 36 deg were scanned to emphasize the impact of transition on the maximum lift coefficient. Here again, a good agreement is observed and no significant difference can be observed between fully turbulent computations and computations with transition in the linear part of the C_L curve. The small effect of transition on C_L in the linear part implies that the lift-induced drag and the pressure drag coefficients, which are preponderant for high-lift configurations [27], remain nearly unchanged in that case. It should also remind one that the main body of the wing is fully turbulent. This explains the small sensitivity of drag coefficient to the transition observed in that case between turbulent and transitional computations. Concerning the maximum lift region, one can observe a significant effect of transition leading to a better estimation compared with fully turbulent results. The agreement on the lift slope is also improved. Some small differences remain for the estimation of the angle of attack corresponding to the maximum lift coefficient. This small discrepancy can come from the

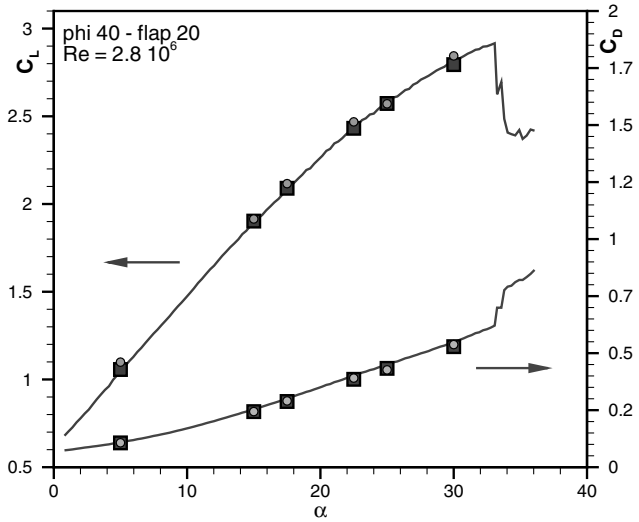

a) M = 0.2, $Re_c = 2.8 \times 10^6$. Squared symbols : fully turbulent computations, Circles : computations with transition, Solid lines : experimental results.

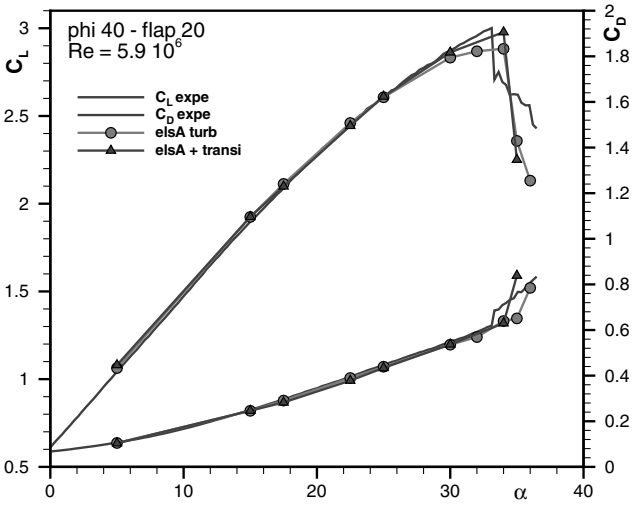

b) M = 0.2, $Re_c = 5.9 \times 10^6$. Circles : fully turbulent computations, Triangles : computations with transition, Solid lines : experimental results.

Fig. 9 $C_L(\alpha)$ and $C_D(\alpha)$ curves. Effect of transition internally computed in the elsA solver. Comparison with experiments.

Table 3 Evolution of the transition location with the Reynolds number; upper side of the slat at $\alpha = 15$ deg; comparison with experimental data

Re_c	2.8×10^6	4.65×10^6	5.9×10^6
X_T/c exper.	0.08	0.06	0.04
X_T/c elsA	0.06	0.05	0.03

experimental setting which was dedicated to the observation of transition rather than the measurement of performances. Electric cables for hot films were gathered at the tip of the wing, which could have affected the stall mechanism.

2. Reynolds Number Effect at $\alpha = 15$ deg

Table 3 shows the evolution of the transition location on the suction side of the slat with the Reynolds number and a comparison to experimental results. The Reynolds number effect is well reproduced. In the experiment, transition locations were measured mainly at 15 deg angle of attack by hot film gauges. The distance between the films is around 2% of the chord in the transition region. This leads to an uncertainty in the estimate of the experimental transition location on the order of $\pm 1\%$ of the chord. The comparison between the experimental and computed transition locations shows a good agreement. Nevertheless, the systematic difference between the experimental and the computed results could be due to the slight overestimation of the integral thicknesses in elsA. A comparison on the pressure distribution is plotted in Fig. 10. One can conclude that the variation in Reynolds number has no significant effect on the pressure distribution.

IV. Conclusions

A new implementation of transition criteria based on the computation line concept was introduced in the elsA Navier–Stokes solver to get rid of most of the mesh topology limitations. Validations on 2-D and 3-D test cases gave encouraging results. Further improvements concerning the stability computations, robustness, and accuracy were also achieved and allowed the authors to explore a larger range of aerodynamic conditions, like the range of angles of attack treated for the Somers laminar airfoil, without any convergence problem. The gathering of two criteria, the Arnal–Habiballah–Delcourt and the Gleyzes–Habiballah criteria, allowed the transition location in the case of separated bubbles to be computed. The effect of transition on maximum lift coefficient was also emphasized for a high-lift configuration. Further computations will have to be carried out for the 3-D test case (AFV wing) to take transition triggered by crossflow instabilities into account. Limitations of the model appear when considering transition computation on a fuselage, because transition criteria need to be applied along the streamlines and not along the mesh lines as it is coded in the actual version. Nevertheless, the object-oriented programming strategy that was introduced allows the introduction of the streamlines computation without modifying the existing implementation. The transmission of information for transition computation through partly or noncoinciding joints between domains should also be considered.

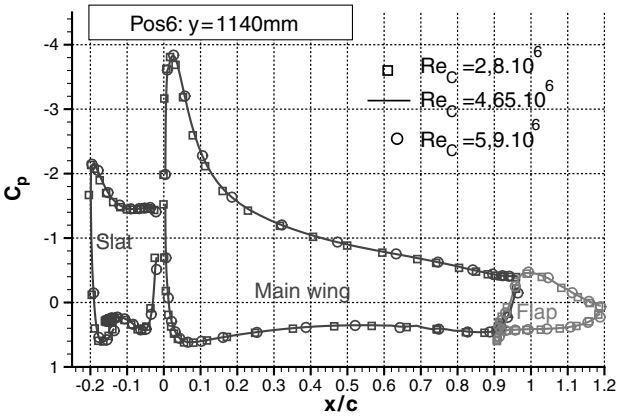

Fig. 10 Reynolds number effect on the C_p distribution at midspan, $\alpha = 15$ deg.

References

[1] Wilcox, D., "Simulation of Transition with a Two-Equation Turbulence Model," *AIAA Journal*, Vol. 32, Feb. 1994, pp. 247–255.

[2] Menter, F., Esch, T., and Kubacki, S., "Transition Modeling Based on Local Variables," *5th International Symposium on Engineering Turbulence Modelling and Measurements*, 2002.

[3] Menter, F., Langtry, R., Likki, S., Suzen, Y., Huang, P., and Völker, S., "A Correlation-Based Transition Model using Local Variables Part 2: Model Formulation," *ASME Turbo Expo 2004 Power for Land, See and Air*, American Society of Mechanical Engineers GT2004-53452, 2004.

[4] Langtry, R., Menter, F., Likki, S., Suzen, Y., Huang, P., and Völker, S., "A Correlation-Based Transition Model Using Local Variables Part 2: Test Cases and Industrial Applications," *ASME Turbo Expo 2004 Power for Land, See and Air*, American Society of Mechanical Engineers, GT2004-53454, 2004.

[5] Langtry, R., and Menter, F., "Transition Modeling for General CFD Applications in Aeronautics," AIAA Paper 2005-522, 2005.

[6] Krumbein, A., "On Modeling of Transitional Flow and its Application on a High Lift Multi-Element Airfoil Configuration," *41st Aerospace Sciences Meeting and Exhibit*, AIAA 2003-724, Jan. 2003.

[7] Cliquet, J., and Houdeville, R., "New Developments in Transition Computation in the elsA Navier–Stokes Solver," *7th ONERA-DLR Aerospace Symposium (ODAS)*, Oct. 2006.

[8] Hansen, H., Thiede, P., Rudnik, R., Moens, F., and Quest, J., "Overview About the European High Lift Research Programme EUROLIFT," *42nd AIAA Aerospace Sciences Meeting and Exhibit*, AIAA Paper 2004-767, Jan. 2004.

[9] Cambier, L., and Gazaix, M., "elsA: An Efficient Object-Oriented Solution to CFD Complexity," *40th AIAA Aerospace Sciences Meeting & Exhibit*, AIAA Paper 2002-0108, Jan. 2002.

[10] Stock, H., and Haase, W., "Feasibility Study of e^N Transition Prediction Method in Navier–Stokes Methods for Airfoils," *AIAA Journal*, Vol. 37, No. 10, 1999, pp. 1187–1196.

[11] Smith, A. M. O., and Gamberoni, N., "Transition, Pressure Gradient and Stability Theory," Douglas Aircraft Co., Rept. ES 26 388, 1956.

[12] van Ingen, J. L., "A Suggested Semi-Empirical Method for the Calculation of the Boundary Layer Transition Region," Delft Univ. of Technology, Dept. of Aeronautic Engineering, Rept. UTH-74, Delft, The Netherlands, 1956.

[13] Mack, L. M., Transition and Laminar Instability Theory, Jet Propulsion Lab. Publ. 77-15 Pasadena, CA, 1956.

[14] Arnal, D., "Special Course on Stability and Transition of Laminar Flow," AGARD Special Course at the von Kármán Inst., AGARD Rept. No. 709, 26–30 March 1984.

[15] Granville, P. S., "Calculation of the Viscous Drag of Bodies of Revolution," David Taylor Model Basin Rept. 849, 1953.

[16] Gleyzes, C., Cousteix, J., and Bonnet, J. L., "Theoretical and Experimental Study of Low Reynolds Number Transitional Separation Bubbles," *Conference on Low Reynolds Number Airfoil Aerodynamics*, Univ. of Notre Dame, Notre Dame, IN, 1985.

[17] Habiballah, M., "Analyse de l'instabilité des Couches Limites Laminaires et Prévision de la Transition du Régime Laminaire au Régime Turbulent," Ph.D. Thesis, École Nationale Supérieure de l'Aéronautique et de l'Espace, Toulouse, France, June 1981.

[18] Somers, D. M., "Design and Experimental Results for a Natural-Laminar-Flow Airfoil for General Aviation Applications," NASA TP 1861, Scientific and Technical Information Branch, 1981.

[19] Gaible, F., Cariou, R., and Houdeville, R., "Numerical Simulation of Three-Dimensional Supersonic Flows Using Euler and Boundary-Layer Solvers," *31th AIAA Aerospace Sciences Meeting & Exhibit*, AIAA 93-0531, Jan. 1997.

[20] Houdeville, R., "Three-Dimensional Boundary-Layer Calculation by a Characteristic Method," *Fifth Symposium on Numerical and Physical Aspects of Aerodynamic Flows*, Jan. 1992.

[21] Manie, F., Piccin, O., and Ray, J., "Test Report of the 2-D Model M1 in the ONERA F1 Wind Tunnel," Group for Aeronautical Research and Technology in Europe High-Lift Action Group AD (AG-08),TP041, Oct. 1989.

[22] Arthur, M., Dol, H., Krumbein, A., Houdeville, R., and Ponsin, J., "Application of Transition Criteria in Navier–Stokes Computations," GARTEUR TP-137, Jan. 2003.

[23] Smith, B., "Near Wall Model for the $k - l$ Two Equation Turbulence Model," *25th Fluid Dynamics Conference*, AIAA Paper 94-2386, June 1994.

[24] Arnal, D., "Transition Prediction in Transonic Flow," *IUTAM Symposium Transsonicum III DFVLR-AVA*, Springer–Verlag, Berlin, 1988, pp. 253–262.

[25] Séraudie, A., Perraud, J., and Moens, F., "Transition Measurements and Analysis on a Swept Wing in High-Lift Configuration," *Aerospace Science and Technology*, Vol. 7, No. 8, 2003, pp. 569–576. doi:10.1016/j.ast.2003.04.001

[26] Perraud, J., Séraudie, A., and Moens, F., "Transition on a High-Lift Swept Wing in the European Project EUROLIFT," *Journal of Aircraft*, Vol. 41, No. 5, 2004, pp. 1183–1190.

[27] Toulorge, T., Ponsin, J., Perraud, J., and Moens, F., "Automatic Transition Prediction for RANS Computations Applied to a Generic High-Lift Wing," *45th AIAA Aerospace Sciences Meeting & Exhibit*, AIAA 07-1086, 2007.

C. Bailly
Associate Editor